MULTI-RESPONSE OPTIMIZATION BASED FRICTION STIR WELDING PROCESS PARAMETERS SETTINGS FOR ALUMINUM ALLOYS

Appasaheb N. Pandav[1,2] , Ratan A. Patil[2], Suman Pandipati[3]
[1]Amity University Maharashtra, Panvel, Mumbai Maharashtra -410206, India.
[2] Jain College of Engineering, Department of Mechanical Engineering
Belgaum, Karnataka-590014, India
[3] Aditya Institute of Technology and Management, Department of Mechanical Engineering
Tekkali, Andhra Pradesh-532203, India
Corresponding author: Appasaheb N. Pandav (appu.pandav@gmail.com)
Mob: +91-8975062699

Abstract:

This study aims at the optimization of friction stir welding (FSW) process parameters by using a Taguchi-grey relational analysis and principal component analysis. The work used several analytical methods to identify the optimal combination of parameters for superior weld characteristics that can enhance the performance and reliability of aluminum-lithium alloy components in security and aviation environments. The combination of PCA with the conventional Taguchi-GRA methodology allows for a detailed analysis of response significance. In total, 16 experiments were conducted using a Taguchi L16 orthogonal array. The performance and quality of each welded joint produced were subjected to rigorous evaluation tests, including tensile strength, yield strength, percentage elongation, weld zone hardness, heat-affected zone hardness, bending load, and the width of the heat-affected zone. From the Taguchi-GRA-PCA analysis, the deduced optimum process parameters were found to be a traverse speed of 160 mm/min, a tilt angle of 200, a rotational speed at 900 rpm, and a shoulder diameter of 16 mm. However, of all the five, the rotational speed was the one contributing more significantly, 43.56% in determining the final result. This means that small variation in the speed of rotation has a huge impact on the quality of welds.

Keywords: Taguchi Analysis; grey relational method; orthogonal array; variance analysis.

1. Introduction

The third generation of aluminum-lithium alloys has been designed and innovatively engineered in such a way that these alloys specifically tackle and surmount the myriad shortcomings and constraints that were notably prevalent in the second-generation alloys and thus elevate their performance standards. This advancement not only enhances their capabilities but enables them to robustly compete with composite materials across a diverse spectrum of applications in various industries. A quintessential example is widely used AA 2050, which offers very good applicability to the defence sectors because

of its attractive features. This alloy is highly valued due to its superior strength-to-weight ratio, which far surpasses many other alternatives; significantly improved fracture toughness, excellent resistance to corrosive environments, and exceptional ability to consistently retain mechanical properties in all orientations, thereby making it a reliable option for applications that require high performance and durability [1-2]. Although fusion welding inherently has some disadvantages, including cracking, incidence of porosity, and problems of distortion, embrittlement, and loss of integrity to the alloy, it may be worth mentioning that FSW is a niche process among the solid-state welds. It involves a pinned shoulder and shoulder, which has a part of the projecting pin less in width than the welding plate, thus creating entirely new process of material joining. It is possible to state that the developed process should be referred to as the technique of extrusion-based kind where a controlled process of generation of heat arises from the normal pressure and shear imposed by a shoulder. In this novel welding process, the frictional heat generated is used to soften the material, and then the softened material flows easily between the tool pin and areas of the material that are not deformed. Therefore, the final joint of this welding method has good quality and strength, so FSW is a highly preferred and advantageous method for various applications in many industries [3].

Taguchi methodology has been applied extensively and rigorously in the optimization of process parameters, mostly with respect to a single response variable. In the very detailed study made by Jayaraman et al. [4], process constraints that are very integral to the FSW of cast aluminum alloy A319 were optimized as the main focus. In one such significant discovery, the researchers found that a precise combination of parameters, specifically rotational speed calibrated at 1200 rpm, traverse speed finely tuned to 40 mm/min, and axial force set at 4 kN, resulted in the highest tensile strength that was recorded in their series of experiments. Similarly, Muralikrishna et al. [5] performed an optimization of process parameters for the FSW of dissimilar aluminum alloys AA2024 and AA6351 with the assistance of rotational speed, traverse speed, and axial force. In a parallel vein, Kumar et al. [6] carried out an optimization study that aimed at refining and enhancing the process parameters associated with the FSW of dissimilar aluminum alloys AA6061 and AA6082. K Lenin and his dedicated research team [7] have made a noteworthy contribution by thoroughly investigating the optimization of process parameters for the FSW of polypropylene material. The underlying principle was to improve the inherent characteristics of tensile strength, hardness, and impact strength through systematic determination of optimum traverse speed, rotational speed, and specific tool pin profile. In another related study, Raweni [8] focused on the process parameters optimization for FSW of AA5083 aluminum alloy. The central objective of the research was to exploit the energy required for the initiation and propagation of cracks, being a critical factor in the long-term durability and reliability of welded joints in practical applications. Sahu [9] conducted a very in-depth study using the Taguchi-based GRA methodology during the course of their research work, with the ultimate goal of optimizing the various process parameters involved in the FSW of the magnesium alloy named AM20. In this integrated

assessment, they accurately evaluated and examined numerous factors, among them being tool rotational speed, welding travel speed, diameter of the shoulder, as well as the plunge depth.

Kundu [10] made significant advancements concerning the process parameters utilized for the FSW of the aluminum alloy designated AA5083. Within the framework of their research, they concentrated on the maximization of the grey relational grade, which is fundamentally a key indicator reflecting the quality characteristics associated with tensile strength, percentage elongation, and micro-hardness of the welded joints produced. Sundar et al. [11] successfully identified the optimal process parameters necessary for the Friction Stir Welding of various titanium-magnesium (Ti-Mg) alloy combinations, while placing a pronounced emphasis on addressing multiple response variables. The general objective of their work was to enhance the strength and quality of the welds significantly with proper selection and optimization of parameters such that the desired mechanical properties could be achieved finally. Furthermore, Mehat [12] cleverly applied PCA to draw objective weight values, which indeed minimized the degree of subjectivity that is generally found in the process of assigning weights towards various responses. This new and systematic approach enabled an eminently more precise determination of the process parameters engaged, thus ultimately leading to enhanced optimization results that could be obtained with the analysis performed. In another study, Paper [13], the authors considered a hybrid approach that precisely combined the Taguchi approach with GRA to optimize the process parameters relevant to friction stir spot welding of the aluminium alloy known as AA2219. The technique proved very effective in enhancing the quality of the welded joints, indicating outstanding versatility and applicability of the hybrid approach in welding processes optimization across a broad range of aluminum alloys. This theme continues, when Li et al. [14] approached a new venture by bringing together Taguchi-based GRA and kernel principal component analysis in an effort to optimize process parameters, which are associated with the turning operation of the titanium alloy Ti-6Al-4V. This new combination of techniques has offered a better insight into the numerous factors that influence the turning process, which ultimately leads to enhanced results with improved precision and operational efficiency. The paper [15] tries to enhance the effectiveness of the FSW process through proper implementation of Taguchi and ANOVA techniques, which are highly acclaimed for their high performance in optimizing intricate industrial processes. In a separate study titled [16], the overall performance of Friction Stir Welding was comprehensively assessed as regards to industrial-grade steel pipes produced from AISI316L and P91 material, thus offering insight into how the above materials perform under welding conditions. 1. The work cited as [17] is mainly focused on improving mechanical properties and temperature distribution of friction stir welds made in aluminum alloys AA6061 and AA6082, so that there is a marked enhancement in performance characteristics. Moreover, the work [18] is targeted towards optimizing the friction stir process parameters with respect to AA6063 by widely recognized Taguchi method.

The prime objective of the research study as appeared in [19] would be the complicated task concerning optimization of various process parameters involved in the friction stir welding technique

that has come to be applied to such dissimilar aluminum alloys as those prominent AA 6061-T6 and AA 5083-H111, all such optimization through sophisticated methodology, Grey relation analysis methodology. In order to critically examine the microstructural properties and to clearly detect any possible welding defects that can occur in the process, a state-of-the-art scanning electron microscope was utilized as an important analytical tool. The process referred to as FSW is widely and frequently used by the industry in joining the various aluminum alloys, as cited in reference [20]. However, the implementation of this method brings up some residual stresses within the materials welded, which means a significant risk to the overall integrity and reliability of the components manufactured using this welding process. The focus of the work presented in [21] is placed on increasing and optimizing FSSW parameters, which in this case are applied specifically with AA1230 aluminum alloy, with a monitoring system for real-time evaluation of axial load imposed by the tool and welding temperature in the process. The research outlined in the paper identified as [22] delves into the fractural characteristics exhibited by an aluminum/steel joint that was created through the process of friction stir welding, with particular attention given to the formation and characteristics of intermetallic compounds and the pivotal influence that a brittle intermetallic layer has on both the initiation and propagation of cracks within the joint. The principal objective of the studies referenced in [23-24] is to meticulously identify the most favorable process parameters for the friction stir welding of the aluminum 2024 alloy, utilizing a comprehensive multi-criteria decision-making framework that encompasses a series of experimental investigations, alongside methodologies such as Grey Relational Analysis and the Technique for Order Preference by Similarity to Ideal Solution. The work [25] introduces an innovative three-step friction stir riveting (FSR) technique, which is specifically designed to effectively join aluminum alloy sheets with high-strength steel sheets robustly. The AA2050 aluminum-lithium alloy is particularly renowned for its remarkable strength-to-weight ratio, exceptional fatigue resistance, and outstanding corrosion resistance properties, thereby rendering it exceptionally well-suited for aerospace applications where the critical objective is to minimize weight while simultaneously ensuring the maintenance of strength. The selection of AA2050 over the alternatives AA2024 and AA7050 was made primarily due to its advantageous characteristics, which include lower density and superior corrosion resistance, as highlighted in references [26-28].

The research indicated in [29] centers on the optimization of various process parameters that are essential for achieving specific quality benchmarks concerning both tensile strength and hardness strength levels. To conduct this analysis, specimens were carefully extracted from a 5 mm thick sheet of 6061-T6 aluminum alloy that was configured in a butt joint arrangement, allowing for a comprehensive examination of the welding process. The analysis performed in reference [30] meticulously examined three critical welding parameters, namely tool rotational speed, traverse speed, and tool axial force, across a range of different levels, which ultimately led to the development of precise and significant predictive models for accurately forecasting the characteristics of the welded joints. In the study [31], response surface methodology was employed as a sophisticated tool to forecast and

subsequently enhance the tensile properties of friction stir welds that were executed on the AA 7020 aluminum alloy. The commercial A7020-T6 plates underwent a series of friction stir welding operations at varying rotational speeds, which had a direct influence on the welding heat input, the resulting microstructure, and the mechanical properties of the welded joints, as thoroughly discussed in reference [32]. A central composite rotatable design was utilized in [33] to create a mathematical model that is specifically aimed at predicting the tensile properties of joints that were friction stir welded from AA 6061-T4 aluminum alloy, achieving an impressive confidence level of 95% in the predictions made by the model. The scholarly investigation presented in reference [34] meticulously delves into the multifaceted effects exerted by various parameters including tool rotational speed, tool traverse speed, and the specific zinc content incorporated within the material matrix on the resultant grain size and hardness characteristics of friction-stir-welded copper-zinc (Cu-Zn) alloys, thereby providing a comprehensive understanding of these influential factors. In furtherance of this research domain, a sophisticated fuzzy logic model was innovatively proposed in reference [35], aimed specifically at the optimization of the friction stir welding process pertinent to pure copper, which consequently led to marked enhancements in the joint properties, most notably including the ultimate tensile strength (UTS) and the elongation capacity, thereby indicating significant improvements in the mechanical performance of the welded joints. It is noteworthy that the hybrid Taguchi- GRA and PCA methodology has been applied with relative infrequency within the context of friction stir welding operations, specifically aiming to augment the process parameters associated with the AA2050 aluminum alloy, which underscores the potential for further research in this area. Predominantly, most methodologies derived from Taguchi or Taguchi-GRA frameworks tend to focus their analytical efforts on a rather constrained number of weld quality parameters, as indicated in reference [36], with such investigations typically limiting their scope to not more than three critical parameters. To systematically structure the experimental design, a Taguchi L16 orthogonal array was employed, as detailed in reference [37], with the primary factors under scrutiny encompassing traverse speed, rotational speed, shoulder diameter, tilt angle, and the configuration of the tool pin, thereby facilitating a comprehensive examination of these variables in the welding process.

2. Materials and Methods

2.1. Experimental design

It is required to conduct 4^5 trials to analyze all potential combinations of five factors with four levels each in a full factorial design. To enhance efficiency in terms of time and cost, Taguchi fractional factorial design was utilized, concentrating on significant combinations. The L16 orthogonal array (OA) was established with sixteen runs using the MINITAB 17 software. The specific variables and their corresponding levels can be found in Table 1. Furthermore, Figure 1 displays the designated tool pin strategies.

2.2. Multi-response optimization using Taguchi-based GRA and PCA

The Taguchi method is employed to identify the optimal parameters for a given process, taking into account a designated performance metric. The Taguchi-based GRA approach is suitable for situations involving multiple responses with varying performance attributes. By incorporating PCA, the ideal weights for these responses are assigned objectively.

2.2.1. Signal-to-noise (S/N) ratios in Taguchi method

The Taguchi methodology employs experimental design techniques to pinpoint the primary sources of variation, which assists in the reduction of variance. The process improvement framework consists of three distinct phases: system design, parameter design, and tolerance design. Within this methodology, S/N ratios serve as indicators of quality. The input variables that cannot be controlled within the system are designated as noise factors. The S/N ratio is expressed as a logarithmic function that takes into account both the average response value and the variability caused by noise. Signal-to-noise analysis classifies quality attributes into three categories: smaller-the-better (STB), larger-the-better (LTB), and nominal-the-best (NBT).

$$\left(\frac{S}{N}\right)_{NBT} = 10\log\left(\frac{y^2}{s^2} - \frac{1}{n}\right) \tag{1}$$

$$\left(\frac{S}{N}\right)_{NBT} = -10\log\left(\frac{1}{n}\sum_{i=1}^{n}\frac{1}{y_i^2}\right) \tag{2}$$

$$\left(\frac{S}{N}\right)_{SBT} = -10\log\left(\frac{1}{n}\sum_{i=1}^{n}y_i^2\right) \tag{3}$$

Improving the signal-to-noise ratio is crucial for all types of performance attributes. In this context, 'n' signifies the number of trials, 'y_i' indicates the response value for the i^{th} iteration of the orthogonal array, 'y^2' represents the mean, and 's^2' refers to the variance of the data.

2.2.2. GRA

The GRA model is widely utilized within the framework of grey system theory. Grey systems frequently suffer from insufficient data points and descriptions, which makes conventional statistical assumptions unsuitable. Handling multiple responses introduces ambiguity due to the conflicting nature of performance attributes. To address this issue, the experimental data concerning performance attributes are normalized to a range between 0 and 1 during the grey relational generation process. Equations (4), (5), and (6) are employed to standardize the performance characteristics for scenarios where the objectives are categorized as LTB, STB, or NBT.

$$xS_i(j) = \frac{x_i(j) - \min x_i(j)}{\max x_i(j) - \min x_i(j)} \tag{4}$$

$$xS_i(j) = \frac{\max x_i(j) - x_i(j)}{\max x_i(j) - \min x_i(j)} \tag{5}$$

$$xS_i(j) = 1 - \frac{\left|x_i(j) - x(j)\right|}{\max\left(\max x_i(j) - x(j), x(j) - \min x_i(j)\right)} \tag{6}$$

The independent and reference values of j[th] enabler's are x(j) and $x_i(j)$.

2.2.3. Measurement of GRA coefficient

Following the standardization of the sequence, the deviation order from the reference order is determined using equation (7).

$$\Delta x_i(j) = \left|x_0(j) - xs_i(j)\right| \tag{7}$$

The deviation sequence is represented as $\Delta x_i(j)$, while the reference arrangement is indicated by $x_0(j)$, and the comparability sequence is denoted as $xs_i(j)$.

$$\xi_i(j) = \frac{\Delta\min + p\Delta\max}{\Delta x_i(j) + p\Delta\max} \tag{8}$$

The 'min' and 'max' deviations of performance features are Δmin and Δmax. The identifying factor, represented by p, can assume values ranging from 0 and 1.

2.2.4. PCA

PCA is a statistical process used to accurately quantify the response's weights, which are then used to estimate grey relational grades (GRG). By reducing the data's amplitude, PCA retains the essential information. The main components model acts as a replacement for multiple variables, capturing most of the data's variability. The computation of principal component weights relies on their eigenvalues. The GRC matrix is utilized as:

$$X_i = \begin{bmatrix} X_{11} & X_{12} & \cdots & X_{1n} \\ X_{21} & X_{22} & \cdots & X_{2n} \\ X_{31} & X_{32} & \cdots & X_{31} \\ \vdots & \vdots & \vdots & \vdots \\ X_{m1} & X_{m2} & \cdots & X_{mn} \end{bmatrix} \tag{9}$$

The matrix of correlation coefficients is precisely defined in equation (10). In this equation, the symbol X_i represents the grey relational coefficients associated with the responses. The letter m

represents the overall count of experimental trials, while the letter n signifies the total number of responses.

$$A_{kl} = \left[\frac{\mathrm{Cov}\left(X_i(k), X_i(l)\right)}{\sigma_{Xi}(k), s_{Xk}(l)} \right] \tag{10}$$

The standard deviations associated with the sequences $X_i(k)$ and $X_i(l)$ are represented by $\sigma_{Xi}(k)$ and $\sigma_{Xk}(l)$. The covariance sequence that exists between $X_i(k)$ and $X_i(l)$ is denoted as $Cov(X_i(k), X_i(l))$.

$$\left[A - \lambda I\right] V = 0 \tag{11}$$

Within this framework, I denotes the identity matrix, V represents the eigenvector, λ signifies the eigenvalue, and A corresponds to the correlation matrix. Equation 12 yields the principal components.

$$PC_i = \sum_{i=1}^{n} X_m(i) V \tag{12}$$

The major component, designated as PC_i, plays a vibrant role in the study.

$$w_{k1} = \frac{\lambda_1}{\lambda_1 + \lambda_2 + \cdots + \lambda_n} \tag{13}$$

$$w_{k2} = \frac{\lambda_2}{\lambda_1 + \lambda_2 + \cdots + \lambda_n} \tag{14}$$

$$\vdots$$

$$w_{kn} = \frac{\lambda_n}{\lambda_1 + \lambda_2 + \cdots + \lambda_n} \tag{15}$$

If the majority of response components for a specific major factor are +ve, then the weight's sign is +ve; otherwise, it is -ve.

2.2.5. GRG

By calculating the grey relational constants through GRA and determining the optimal weights for each action attribute, the GRG is obtained by summing the weighted values of the grey relational constants.

$$\gamma_i = \sum_{i=1}^{n} w_k \xi_i(k) \tag{16}$$

The effect of the weight of every performance appearance is represented as w_k, on the GRC denoted as $\xi_i(k)$ affects the GRG of each i[th] test, signified as γ_i.

$$\gamma_{\text{predicted}} = \gamma_{\text{m}} + \sum_{\text{i=1}}^{\text{q}} \left(\gamma_0 - \gamma_{\text{m}} \right) \quad (17)$$

The highest average GRG achievable at the optimal parameter setting is represented by the symbol γ_o, while the mean GRG is represented by γ_m. Additionally, q signifies the number of parameters that have an impact on the GRG.

2.3. Materials and specimens

The AA2050-T84 plates (200mm x 100mm x 4mm) were selected for the experimental investigation. A comprehensive breakdown of the chemical composition of AA2050 can be found in Table 2. To facilitate the joining of the plates, a single pass of FSW was performed using an FN2EV knee-type milling machine by HMT Ltd. in Pinjore, India. A total of sixteen tools, made from AISI H13 tool steel, were utilized.

3. Results and discussion

The FIE-UTES40 universal testing machine was employed to complete the tensile tests in compliance with the specifications of IS1608 (Part-1): 2020. Hardness tests were performed using a Vickers hardness machine with a load of 5 kgf, adhering to the protocols established in IS1501 (Part-1): 2020. Employing a UTM equipped with a bending jig and a 25 mm mandrel, the determination of the bending load leading to crack formation was carried out as per the specifications of IS 1599: 2019. The width of the heat-affected zone was assessed using the DEWINTER-1500X inverted metallurgical microscope. The outcomes of the experimental trials were documented in Table 3, while the weld bead macrographs were illustrated in Figure 2.

The data presented in Table 3 was transformed into S/N ratios to enable the Taguchi analysis of the L16 orthogonal array through GRA. The aim was to maximize the responses related to yield strength, tensile strength, hardness, percentage elongation, and bending load, as these attributes were deemed advantageous for the analysis. Conversely, a reduction in the heat-affected zone (HAZ) response width was preferred, as it was viewed as a more favorable characteristic for the calculation of S/N ratios. The division of the section on results and discussion into ten parts was conducted. An investigation was performed on the impact of process factors on individual reactions, highlighting the key parameters in sections 3.1 to 3.7.

3.1. Process parameter's effect on tensile strength

The data from Table 3 was subjected to transformation into S/N ratios using the software application Minitab 17. Utilization of the LTB attribute of the Taguchi methodology was essential in ascertaining the S/N ratios specifically for tensile strength. Additionally, the software Minitab was instrumental in both generating the main effects plot and executing the ANOVA analysis. Figure 3

provides a comprehensive graphical representation of the principal effects plot, which meticulously elucidates the S/N ratios that have been derived from the extensive response data collected during the experimental phase of the study. This detailed graphical depiction serves as a fundamental tool for discerning the relative impact and significance of the various process parameters that were meticulously analyzed throughout the investigation. Furthermore, the graphical representation effectively illustrates the intricate correlation that exists between the calculated S/N ratios and the process constraints, thereby facilitating a deeper understanding of their interrelationships. It is important to highlight that there is a noticeable reduction in the S/N ratio as the rotational speed increases from 900 to 1800 rpm, suggesting a possible inverse relationship. In contrast, a significant improvement in the S/N ratio is observed when the tilt angle rises from a low of 0.5 degrees to a higher value of 2 degrees, indicating a direct correlation between these two factors. A detailed comparative analysis of the various tool pins employed shows that the straight cylindrical tool pin has produced the most advantageous results, as evidenced by the highest S/N ratio recorded, while the taper cylindrical tool pin has demonstrated the least effective performance, as indicated by the lowest S/N ratio. The principal effects plot that elucidates the variations in the S/N ratio is meticulously illustrated in Figure 3, providing a clear visual reference for further examination and interpretation.

3.2. Process parameters effect on yield strength

In a manner analogous to the tensile strength analysis elaborated upon in section 3.1 of this academic discourse, the Taguchi method was employed to exploit the larger-the-better characteristic as a means to meticulously evaluate the yield strength S/N ratios. The primary effects plot, which is meticulously illustrated in Figure 4, serves to reveal the nuanced influence exerted by each distinct process parameter on the resultant S/N ratio values, thereby providing a comprehensive understanding of the interactions involved. Among the diverse array of parameters scrutinized, the rotational speed exhibited the most extensive and pronounced range of S/N ratio values, thereby underscoring its substantial and critical impact on the overall process. In addition to this, both the tilt angle and the shape of the tool pin emerged as significant factors that warrant further investigation and discussion. Furthermore, the analysis of the main effects plot concerning the S/N ratio, as depicted in Figure 3, indicated that the optimal parameter levels were indeed effective in facilitating the attainment of elevated S/N ratios alongside improved yield strength values.

3.3. Process parameter's effect on elongation

Figure 5 provides a detailed illustration of the primary effects plot, which effectively showcases the S/N ratios related to the elongation process. Among the various tool pins analyzed, the straight square tool pin achieved the highest S/N ratio, while the taper cylindrical tool pin recorded the lowest. Additionally, an increase in shoulder diameter from 16 mm to 22 mm was found to correlate positively with a significant rise in the S/N ratio for elongation, indicating a strong relationship between these

factors. Initially, the S/N ratio improved notably as the rotating speed increased from 900 rpm to 1120 rpm, suggesting a beneficial connection between these variables. However, once the rotating speed exceeded the critical point of 1120 rpm, the S/N ratio began to decline as the speed continued to rise, reaching up to 1800 rpm. In contrast, the traverse speed had a minimal impact on the S/N ratio, with only a slight increase observed when the speed was adjusted from 80 mm/min to 160 mm/min, underscoring its limited effect in this scenario.

3.4. Process parameter's effect on weld zone hardness

Figure 6 serves to visually represent the principal impact plot, which delineates the S/N ratios associated with the hardness of the weld zone, thereby providing critical insights into the relationship between these variables. A notable decrease in hardness values was observed concomitantly with an increase in the shoulder diameter, which was measured to transition from a dimension of 16 mm to a more substantial 22 mm. Additionally, an increase in rotational speed, specifically from 900 to 1800 revolutions per minute, was observed to correlate with a notable decrease in hardness levels within the weld zone. Among the various types of tool pins assessed in this research, the straight square tool pins were found to possess the highest hardness properties, in sharp contrast to the taper square tool pins, which showed the lowest hardness values. Initially, the hardness measurements displayed an upward trend as the tilt angle was carefully adjusted between 0.5 and 1 degree; however, a subsequent reduction in hardness was noted when the tilt angle was increased further from 1 to 2 degrees.

3.5. Process parameter's effect on heat-affected zone hardness

Figure 7 serves as a visual representation that delineates the primary effects plot concerning the S/N ratios that are intrinsically linked to the hardness characteristics of the heat-affected zone, thereby providing a comprehensive view of the correlation between these variables. It was observed that the most elevated S/N ratio was documented when utilizing the straight square tool pin configuration, whereas the straight cylindrical tool pin configuration resulted in the least favorable S/N ratio measurements. An important inverse correlation was observed between the S/N ratio and the rotational speed, which increased from 900 to 1800 rpm, highlighting a significant interaction between these variables. In contrast, the S/N ratio showed a marked increase as the traverse speed rose from 80 to 160 mm/min, except for a specific interval between 100 and 125 mm/min, where an anomaly was noted. Moreover, the S/N ratio experienced an increase in correlation with the tilt angle, which varied from 0.5 to 1.5 degrees, before subsequently declining from 1.5 to 2 degrees, thus illustrating a complex relationship between these variables. The shoulder diameter was found to exert a negligible influence on the S/N ratio measurements, particularly when analyzing the values that fell within the range of 16 mm to 20 mm, suggesting a limited effect of this parameter on overall outcomes. Based on the empirical data that has been meticulously illustrated in Figure 6, the optimal parameter levels for the processes that are aimed at attaining superior hardness values within the heat-affected zone have been

conclusively identified as Tool Speed 4 (TS4), Rotational Speed 1 (RS1), Tilt Angle 3 (TA3), Shoulder Diameter 2 (SD2), and Tool Pin Position 2 (TPP2).

3.6. Process parameter's effect on bending load

Figure 8 illustrates the main effects plot, highlighting the variations in S/N ratios across different parameters. The taper square tool pin demonstrated a superior S/N ratio, whereas the other three tool pin designs showed similar minimum S/N ratios. Additionally, increasing the rotational speed from 900 rpm to 1800 rpm led to a reduction in the S/N ratio. The S/N ratio also decreased as the shoulder diameter increased from 16 mm to 20 mm and subsequently to 22 mm. The effect of the tilt angle on the S/N ratio was minimal; it declined as the tilt angle increased from 0.5º to 1º, remained relatively constant between 1º and 1.5º, and then saw another decrease from 1.5º to 2º.

3.7. Process parameters effect on heat-affected zone width

Figure 9 illustrates the primary effects plot concerning the S/N ratio of the HAZ width. This plot demonstrates the variation of the S/N ratio across different parameters. The S/N ratio decreases as the shoulder diameter increases from 16mm to 22mm. Conversely, the S/N ratio shows improvement with an increase in traverse speed from 80mm/min to 125mm/min, followed by a minor reduction from 125mm/min to 160mm/min. The impact of rotational speed and tool pin profile on the S/N ratio appears to be somewhat minimal. Specifically, the S/N ratio declines as rotational speed rises from 900 rpm to 1400 rpm, then experiences an increase from 1400 rpm to 1800 rpm. The lowest S/N ratio is recorded with a straight square tool pin, while the highest is noted with a taper square pin. As shown in Figure 8, the ideal process parameter settings for reducing HAZ width are TS3, RS1, TA1, SD1, and TPP4.

3.8. Optimizing multiple responses with principal component and grey relational analysis

In Table 4, the process of data normalization also referred to as grey relational generation, is used in the S/N ratios of the responses presented. These S/N ratios are indicative of excellence characteristics that adhere to the larger-the-better criterion. To facilitate data pre-processing, equation 4 was employed. Subsequently, the reference sequence obtained was transformed into a deviation sequence through the application of a specific equation. To calculate the GRC, the minimum and maximum limits of the variance patterns corresponding to the various answers were determined using Equation 8. A distinguishing coefficient of 0.5 was utilized in the calculation of the GRCs. In this research, rather than using uniform weights or subjective assessments, the response weights were determined through PCA. This methodology involved applying PCA to the GRC data matrix to identify the response weights. By allocating the ranks among the trial operations, Tables 5-6 were created to assess the overall excellence of the welds. The selected level for each parameter was determined, and the average of these values was computed. For instance, the rotational speed parameter was established at level 3 for the 3rd, 7th,

11th, and 15th experimental runs. Equation 18 was used to calculate the mean from the corresponding overall weld quality data $RS(level\ 3) = 1.298682$.

3.9. Overall Weld Quality with ANOVA

An ANOVA test was performed to assess the relevance and relative impact of each value on the weld quality. The test was conducted with a confidence level of 95%. Results showed that rotational speed has the most significant effect on weld quality, explaining 43.56% of the variation. Following closely was the traverse speed at 26.84%, shoulder diameter at 17.76%, tilt angle at 7.11%, and tool pin profile at 4.73%. Furthermore, all process parameters had p-values below 0.05, signifying an important outcome on weld quality. The high R^2 (93.96%) and R^2_{adj} (88.68%) values indicated a good fit of the developed model.

3.10. Confirmation examination

Following the determination of the most effective parameter levels, the concluding phase of the Taguchi-GRA-PCA investigation involves the prediction as well as the validation of the enhancement of GRG, which serves as the overall indicator of weld quality (shown in Table 7). The expected overall indicator of weld quality is calculated by Equation 17. The weld's microstructure is intricate and greatly influenced by its location within the welded area. Fine grains are present in the nugget zone, while coarsened grains are typically found in the TMAZ and HAZ zones, as illustrated in Figure 10. The friction stir welding tool causes plastic deformation in the Thermo-Mechanically Affected Zone (TMAZ), and the heat generated during the process also impacts the material.

4. Conclusions

This scholarly endeavor is meticulously designed to implement a sophisticated hybrid methodology known as Taguchi-GRA-PCA, which serves to ascertain the most effective amalgamation of progression parameters while simultaneously addressing the complexities associated with multiple responses that may arise during the evaluation process.

- The experimental evaluations were conducted using the Taguchi L16 orthogonal array, and the S/N ratios for each result were carefully examined, allowing for an in-depth analysis of how different parameters influence the specific outcomes generated during the welding process.
- A thorough overall assessment of weld quality values was conducted through the application of the Taguchi-GRA-PCA methodology, which ultimately facilitated the creation of a specialized response chart meticulously tailored to depict the overall weld quality analytically.
- The resulting response chart clarifies that the ideal combination of progression parameters essential for improving performance metrics includes a traverse speed of 160 mm/min, a rotational speed of

900 rpm, a tilt angle of 20°, a shoulder diameter of 16 mm, and a configuration featuring a straight square tool pin.

- The ANOVA conducted on the overall weld quality demonstrated statistically significant results across all parameters assessed, with p-values falling below the critical threshold of 0.05. This indicates a robust level of statistical significance in the findings.
- The validation tests indicated a significant improvement of 19.06% in overall weld quality when utilizing the optimal process parameters identified as TS4, RS1, TA4, SD1, and TPP3. This is in sharp contrast to the initially recommended conditions, which were TS3, RS3, TA1, SD2, and TPP4.
- Comparative analysis indicated that fine-grain structures were discernibly present within the nugget zone when juxtaposed against the TMAZ and the HAZ, highlighting the differences in microstructural characteristics.

Acknowledgement

The authors are thankful to the editor and reviewers for their valuable comments to improve the quality of this manuscript.

Conflict of interest

The authors declare no conflict of interests regarding the publication of this paper.

References

[1]. Dursun, T., and Soutis, C. "Recent developments in advanced aircraft aluminium alloys", *Materials & Design 1980-2015*, **56**, pp. 862–871 (2014). DOI: 10.1016/j.matdes.2013.12.002.

[2]. Alam, M. P. and Sinha, A. N., "Fabrication of third generation Al–Li alloy by friction stir welding: a review", *Sadhana*, **44**(6), pp. 153 (2019). DOI: 10.1007/s12046-019-1139-4.

[3]. Threadgill, P. L., Leonard, A. J., Shercliff, H. R., et al., "Friction stir welding of aluminium alloys", *International Materials Reviews*, **54**(2), pp. 49–93 (2009). DOI: 10.1179/174328009X411136.

[4]. Jayaraman, M., Sivasubramanian, R., Balasubramanian, V., et al., "Optimization of process parameters for friction stir welding of cast aluminium alloy A319 by Taguchi method", *Journal of Scientific & Industrial Research*, **68**, pp. 36-43 (2009). DOI: nopr.niscpr.res.in/handle/123456789/2786.

[5]. Krishna, P. M., Ramanaiah, N., and Rao, K. P., "Optimization of process parameters for friction Stir welding of dissimilar Aluminum alloys (AA2024 -T6 and AA6351-T6) by using Taguchi method ", *International Journal of Industrial Engineering Computations*, **4**(1), pp. 71–81 (2012). DOI: 10.5267/j.ijiec.2012.11.002.

[6]. Kumar, S., Kumar, S., and Kumar, A., "Optimization of process parameters for friction stir welding of joining A6061 and A6082 alloys by Taguchi method", *Proceedings of the Institution of Mechanical Engineers Part C Journal of Mechanical Engineering Science*, **227**(6), pp. 1150–1163 (2012). DOI: 10.1177/0954406212459448.

[7]. Lenin, K., Abdul, S.H., Suresh, K., et al., "Process parameters optimization for friction stir welding of Polypropylene material using Taguchi's approach", *Journal of Scientific & Industrial Research*, **73**, pp. 369-374 (2014). DOI: nopr.niscpr.res.in/handle/123456789/28876.

[8]. Raweni, A., Majstorović, V., Sedmak, A., et al., "Optimization of AA5083 friction stir welding parameters using Taguchi method", *Tehnicki Vjesnik - Technical Gazette*, **25**(3) (2018). DOI: 10.17559/TV-20180123115758.

[9]. Sahu, P. K. and Pal, S., "Multi-response optimization of process parameters in friction stir welded AM20 magnesium alloy by Taguchi grey relational analysis", *Journal of Magnesium and Alloys*, **3**(1), pp. 36–46 (2015). DOI: 10.1016/j.jma.2014.12.002.

[10]. Kundu, J. and Singh, H., "Friction stir welding of AA5083 aluminium alloy: Multi-response optimization using Taguchi-based grey relational analysis", *Advances in Mechanical Engineering*, **8**(11) (2016). DOI: 10.1177/1687814016679277.

[11]. Sivam, S. P. S. S., Saravanan, K., Pradeep, N., et al., "Grey Relational Analysis and ANOVA to determine the optimum process parameters for friction stir welding of TI and MG alloys", *Periodica Polytechnica Mechanical Engineering*, **62**(4), pp. 277–283 (2018). DOI: 10.3311/PPme.12117.

[12]. Mehat, N. M., Kamaruddin, S., and Othman, A. R., "Hybrid integration of Taguchi parametric design, Grey relational analysis, and principal component analysis optimization for plastic gear production", *Chinese Journal of Engineering*, **2014**, pp. 1–11 (2014). DOI: 10.1155/2014/351206.

[13]. Ojo, O. O. and Taban, E., "Hybrid multi-response optimization of friction stir spot welds: failure load, effective bonded size and flash volume as responses", *Sadhana*, **43**(6), (2018). DOI: 10.1007/s12046-018-0882-2.

[14]. Li, N., Chen, Y.J., and Kong, D.D., "Multi-response optimization of Ti-6Al-4V turning operations using Taguchi-based grey relational analysis coupled with kernel principal component analysis", *Advances in Manufacturing*, **7**(2), pp. 142–154 (2019). DOI: 10.1007/s40436-019-00251-8.

[15]. Madani, T., Boukraa, M., Aissani, M., et al., "Experimental investigation and numerical analysis using Taguchi and ANOVA methods for underwater friction stir welding of aluminium alloy 2017 process improvement", *International Journal of Pressure Vessels and Piping*, **201**, pp. 104879 (2023). DOI: 10.1016/j.ijpvp.2022.104879.

[16]. Gain, S., Das, S. K., Acharyya, S. K., et al., "Friction stir welding of industrial grade AISI 316L and P91 steel pipes: A comparative investigation based on mechanical and metallurgical properties", *International Journal of Pressure Vessels and Piping*, **201**, pp. 104865 (2022). DOI: 10.1016/j.ijpvp.2022.104865.

[17]. Kumar, R., Dhami, S. S., and Mishra, R. S., "Optimization of friction stir welding process parameters during joining of aluminum alloys of AA6061 and AA6082", *Materials Today Proceedings*, **45**, pp. 5368–5376 (2021). DOI: 10.1016/j.matpr.2021.01.958.

[18]. Umanath, K., Palanikumar, K., Sankaradass, V., et al., "Optimizations of friction stir welding process parameters of AA6063 Aluminium alloy by Taguchi technique", *Materials Today Proceedings*, **46**, pp. 4008–4013 (2021). DOI: 10.1016/j.matpr.2021.02.539.

[19]. Elatharasan, G., Manikandan, R., and Karthikeyan, G., "Multi-response optimization of process parameters in friction stir welding of dissimilar aluminum alloys by Grey relation analysis (AA 6061-T6 & AA5083-H111)", *Materials Today Proceedings*, **37**, pp. 1172–1182 (2020). DOI: 10.1016/j.matpr.2020.06.353.

[20]. Sabry, N., Stroh, J., and Sediako, D., "Characterization of microstructure and residual stress following the friction stir welding of dissimilar aluminum alloys", *CIRP Journal of Manufacturing Science and Technology*, **41**, pp. 365–379 (2023). DOI: 10.1016/j.cirpj.2022.11.021.

[21]. Al-Sabur, R., Jassim, A. K., and Messele, E., "Real-time monitoring applied to optimize friction stir spot welding joint for AA1230 Al-alloys", *Materials Today Proceedings*, **42**, pp. 2018–2024 (2021). DOI: 10.1016/j.matpr.2020.12.253.

[22]. Beygi, R., Akhavan-Safar, A., Carbas, R., et al., "Utilizing a ductile damage criterion for fracture analysis of a dissimilar aluminum/steel joint made by friction stir welding", *Engineering Fracture Mechanics*, **274**, pp. 108775 (2022). DOI: 10.1016/j.engfracmech.2022.108775.

[23]. Sudhagar, S., Sakthivel, M., Mathew, P. J., et al., "A multi criteria decision making approach for process improvement in friction stir welding of aluminium alloy", *Measurement*, **108**, pp. 1–8 (2017). DOI: 10.1016/j.measurement.2017.05.023.

[24]. Khajeh, R., Jafarian, H. R., Seyedein, S. H., et al., "Microstructure, mechanical and electrical properties of dissimilar friction stir welded 2024 aluminum alloy and copper joints", *Journal of Materials Research and Technology*, **14**, pp. 1945–1957 (2021). DOI: 10.1016/j.jmrt.2021.07.058.

[25]. Shan, H., Ma, Y., Yang, B., et al., "Elucidation of interface joining mechanism of aluminum alloy/dual-phase steel friction stir riveting (FSR) joint", *Journal of Materials Research and Technology*, **25**, pp. 6792–6811 (2023). DOI: 10.1016/j.jmrt.2023.07.146.

[26]. Šibalija, T. V. and Majstorović, V. D., "Advanced Multiresponse Process Optimisation," *Advanced Multiresponse Process Optimisation, Cham: Springer International Publishing*, pp. 1–20 (2016). DOI: 10.1007/978-3-319-19255-0_1.

[27]. Proton, V., Alexis, J., Andrieu, E., et al., "Corrosion and stress corrosion cracking behaviour of 2050 aluminium-lithium alloy joined by friction stir welding (FSW)", *EUROCORR 2012*, 2012, Istanbul, Turkey. HAL Id: hal-04104017. Available: https://hal.science/hal-04104017v1.

[28]. Rssodríguez, A., Calleja, A., De Lacalle, et al., "Burnishing of FSW aluminum Al–CU–Li components", *Metals*, **9**(2), pp. 260 (2019). DOI: 10.3390/met9020260.

[29]. Hotelling, H., "Analysis of a complex of statistical variables into principal components.", *Journal of Educational Psychology*, **24**(6), pp. 417–441 (1933). DOI: 10.1037/h0071325.

[30]. Ilkhichi, A. R., Soufi, R., Hussain, G., et al., "Establishing mathematical models to predict grain size and hardness of the friction Stir-Welded AA 7020 aluminum alloy joints", *Metallurgical and Materials Transactions B*, **46**(1), pp. 357–365 (2014). DOI: 10.1007/s11663-014-0205-x.

[31]. Heidarzadeh, A., Barenji, R. V., Esmaily, M., et al., "Tensile properties of friction stir welds of AA 7020 aluminum alloy", *Transactions of the Indian Institute of Metals*, **68**(5), pp. 757–767 (2015). DOI: 10.1007/s12666-014-0508-2.

[32]. Behzadi, M. A., Ranjbar, K., Dehmolaei, R., et al., "Friction-stir-welded overaged 7020-T6 alloy joint: an investigation on the effect of rotational speed on the microstructure and mechanical properties", *International Journal of Minerals Metallurgy and Materials*, **26**(5), pp. 622–633 (2019). DOI: 10.1007/s12613-019-1770-4.

[33]. Heidarzadeh, A., Khodaverdizadeh, H., Mahmoudi, A., et al., "Tensile behavior of friction stir welded AA 6061-T4 aluminum alloy joints", *Materials & Design (1980-2015)*, **37**, pp. 166–173 (2011). DOI: 10.1016/j.matdes.2011.12.022.

[34]. Heidarzadeh, A. and Saeid, T., "Correlation between process parameters, grain size and hardness of friction-stir-welded Cu–Zn alloys", *Rare Metals*, **37**(5), pp. 388–398 (2016). DOI: 10.1007/s12598-016-0704-9.

[35]. Heidarzadeh, A., Testik, Ö. M., Güleryüz, G., et al., "Development of a fuzzy logic based model to elucidate the effect of FSW parameters on the ultimate tensile strength and elongation of pure copper joints", *Journal of Manufacturing Processes*, **53**, pp. 250–259 (2020). DOI: 10.1016/j.jmapro.2020.02.020.

[36]. Asmare, A., Al-Sabur, R., and Messele, E., "Experimental Investigation of Friction Stir Welding on 6061-T6 Aluminum Alloy using Taguchi-Based GRA", *Metals*, **10**(11), pp. 1480 (2020). DOI: 10.3390/met10111480.
[37]. Asmare, A., Al-Sabur, R., and Messele, E., "Experimental Investigation of Friction Stir Welding on 6061-T6 Aluminum Alloy using Taguchi-Based GRA", *Metals*, **10**(11), pp. 1480 (2020). DOI: 10.3390/met10111480.
[38]. Heidarzadeh, A., Khodaverdizadeh, H., Mahmoudi, A., et al., "Tensile behavior of friction stir welded AA 6061-T4 aluminum alloy joints", *Materials & Design (1980-2015)*, **37**, pp. 166–173 (2011). DOI: 10.1016/j.matdes.2011.12.022.

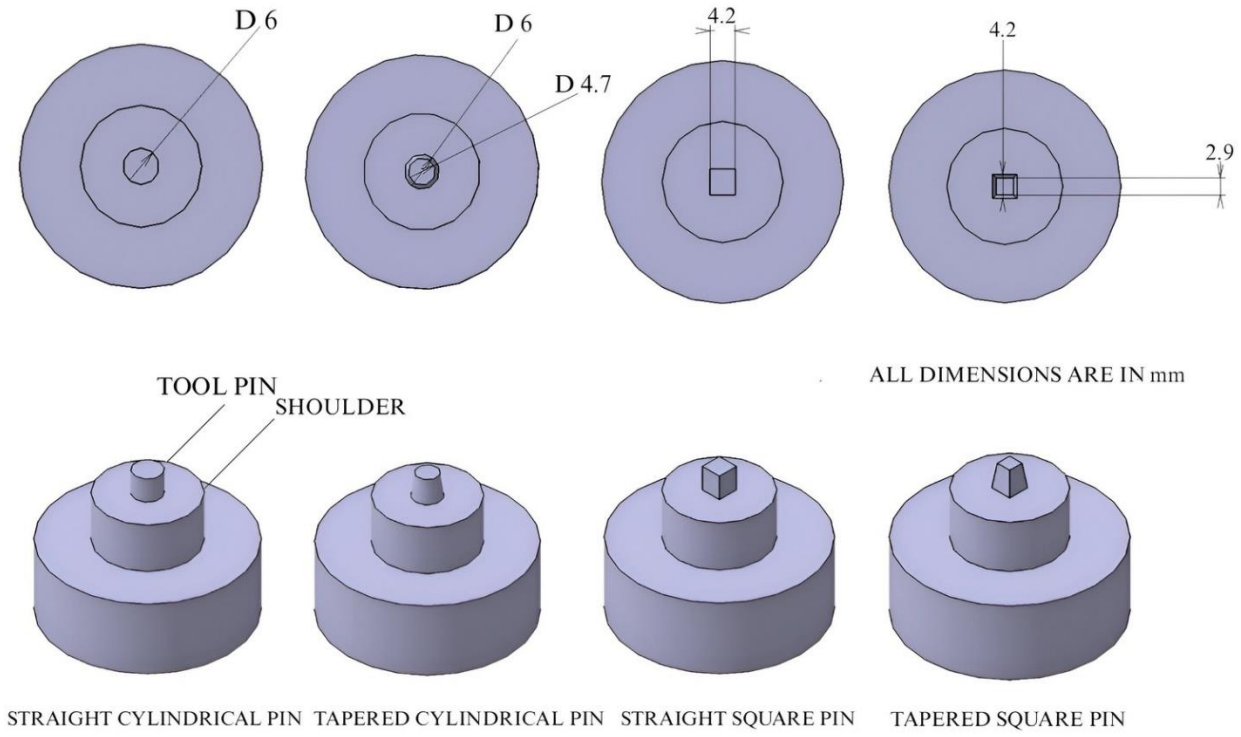

Figure 1. Tool Pin Profiles

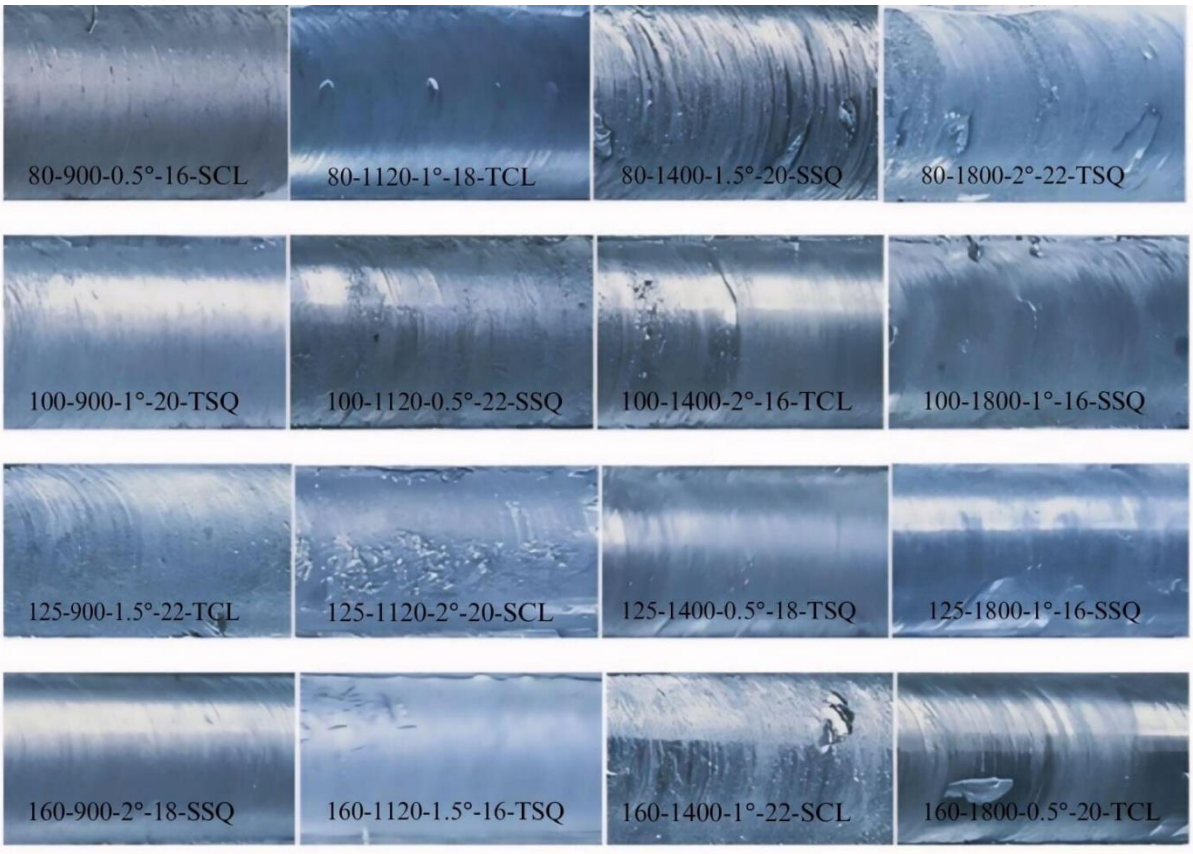

Figure 2. Weld beads macrographs (parameters in the order Traverse Speed (TS)-Rotational speed(RS)-Tilt Angle(TA)-Shoulder Diameter(SD)-Tool Pin Profile(TPP))

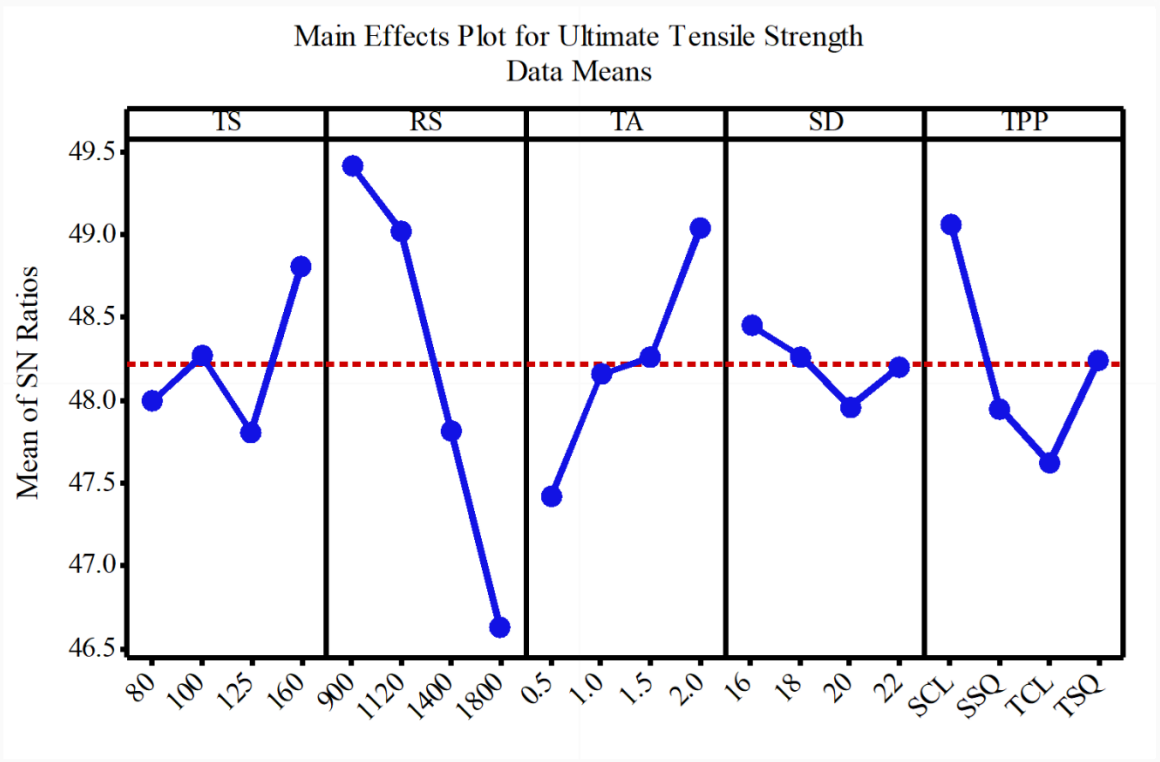

Figure 3. Effects of tensile strength for S/N ratios

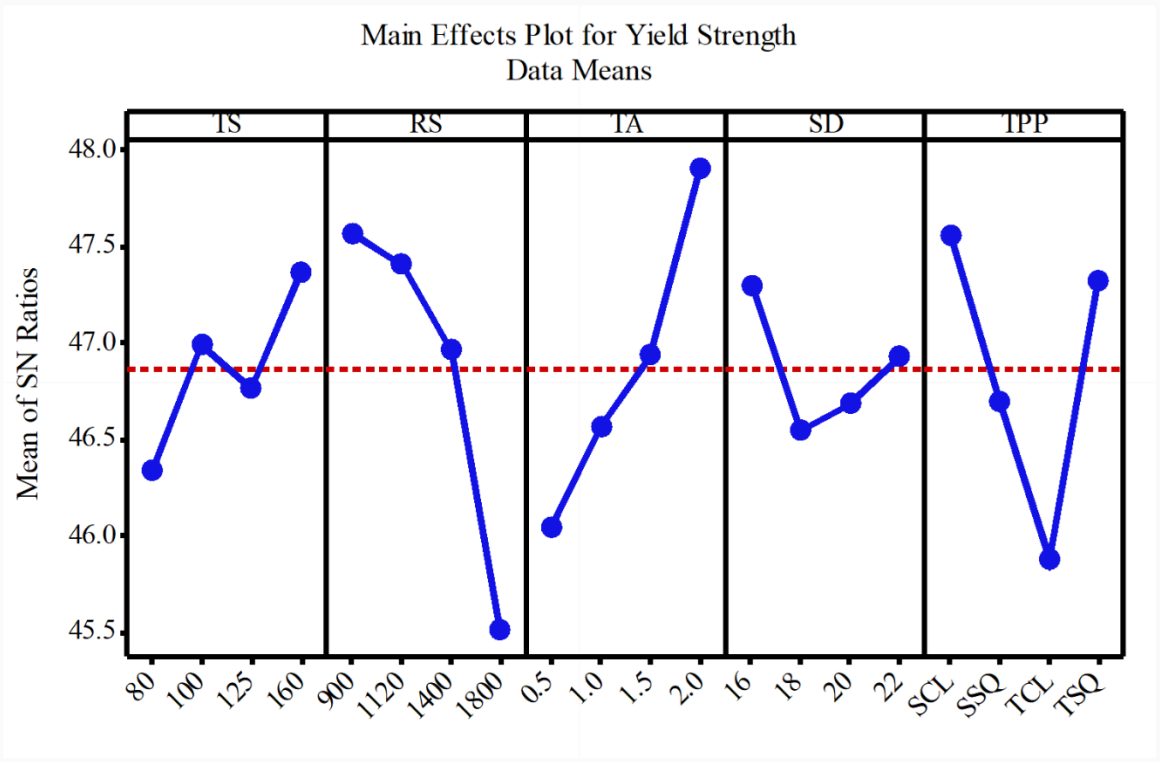

Figure 4. Effects of yield strength for S/N ratios

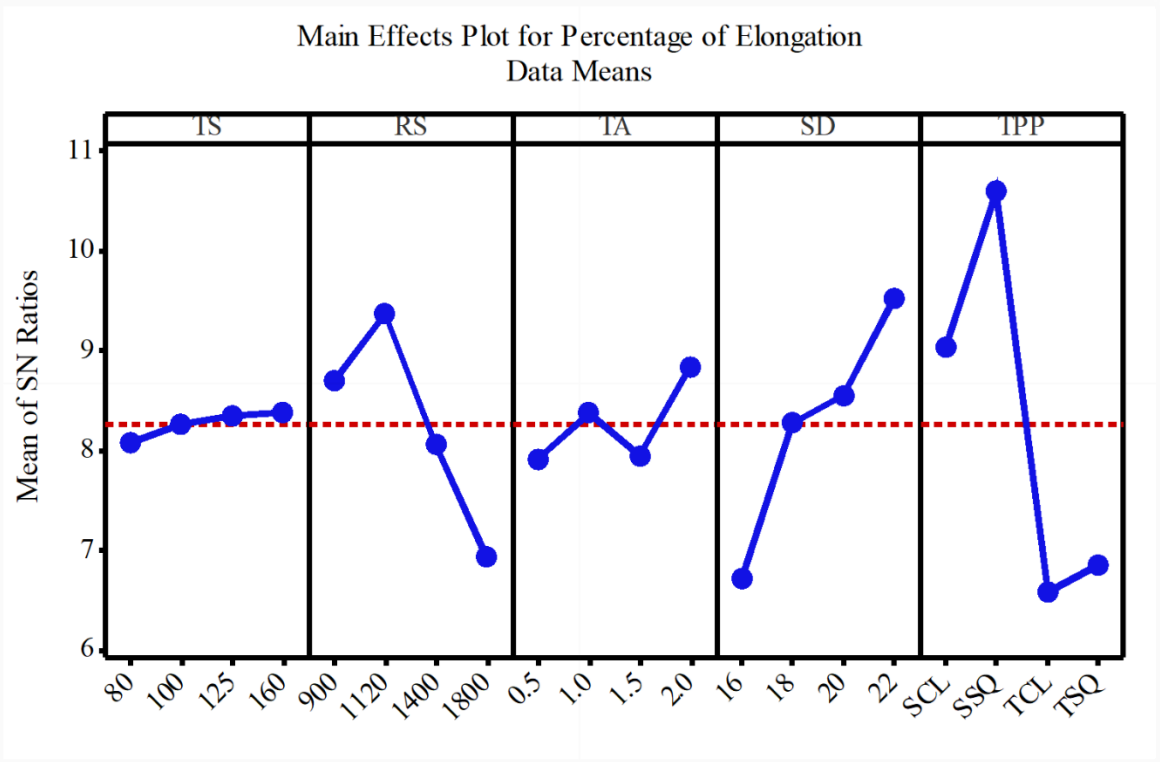

Figure 5. Effects of % elongation for S/N ratios

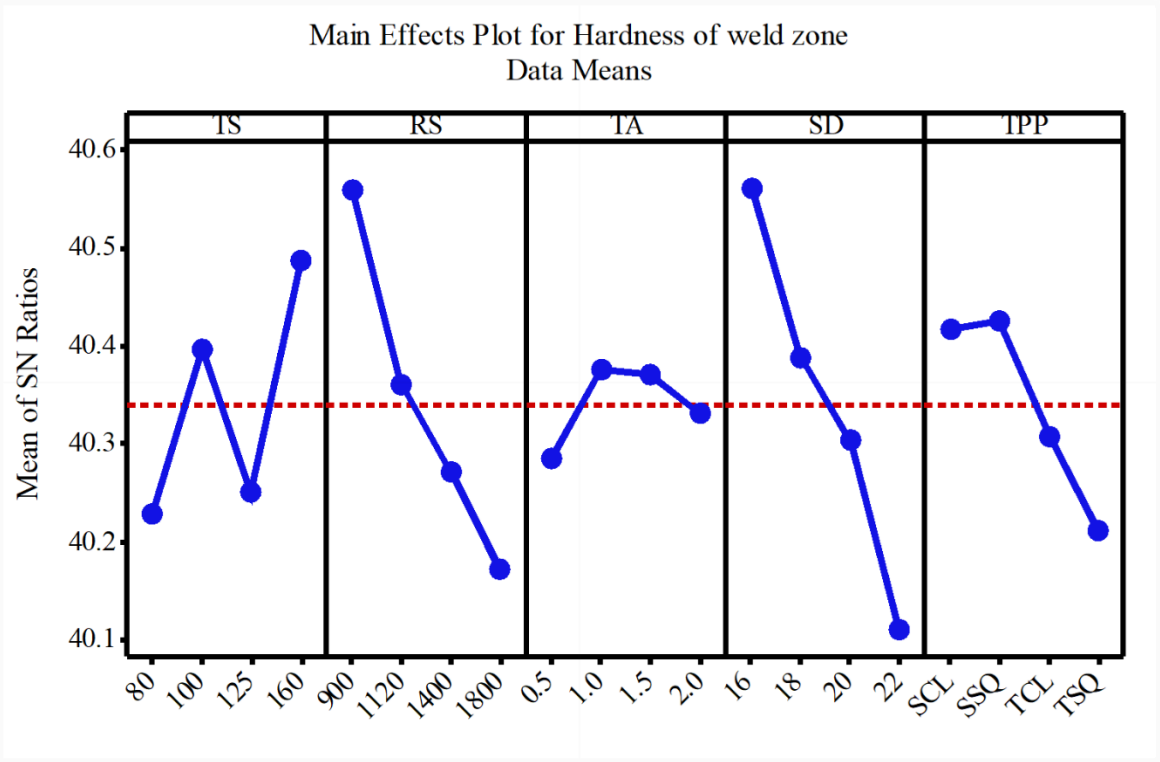

Figure 6. Effects of weld zone hardness for S/N ratios

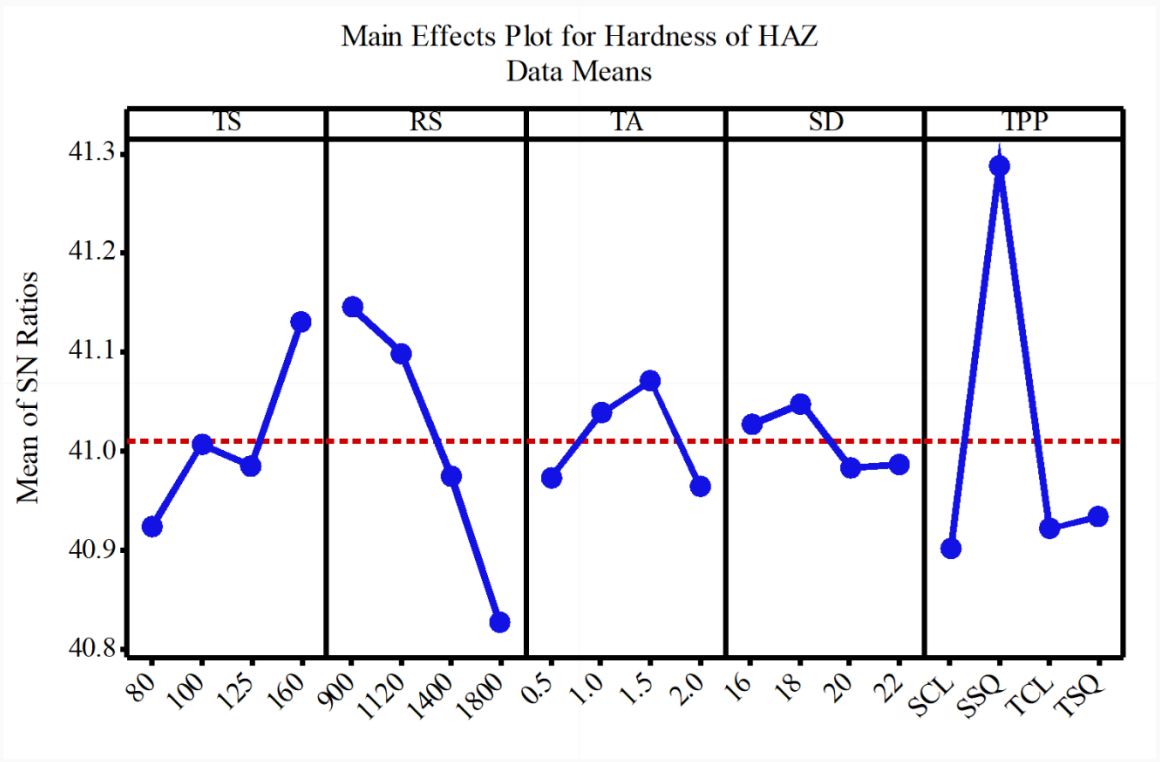

Figure 7. Effects of heat affected zone hardness for S/N ratios

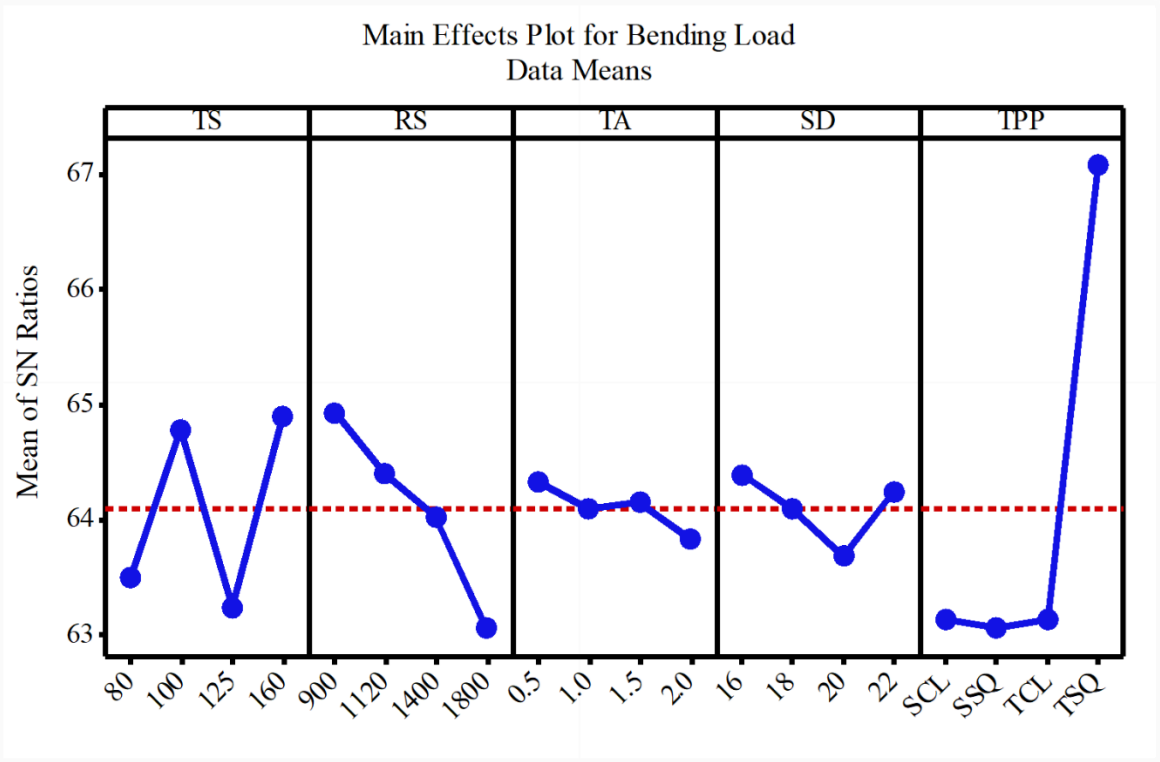

Figure 8. Effects of bending load for S/N ratios

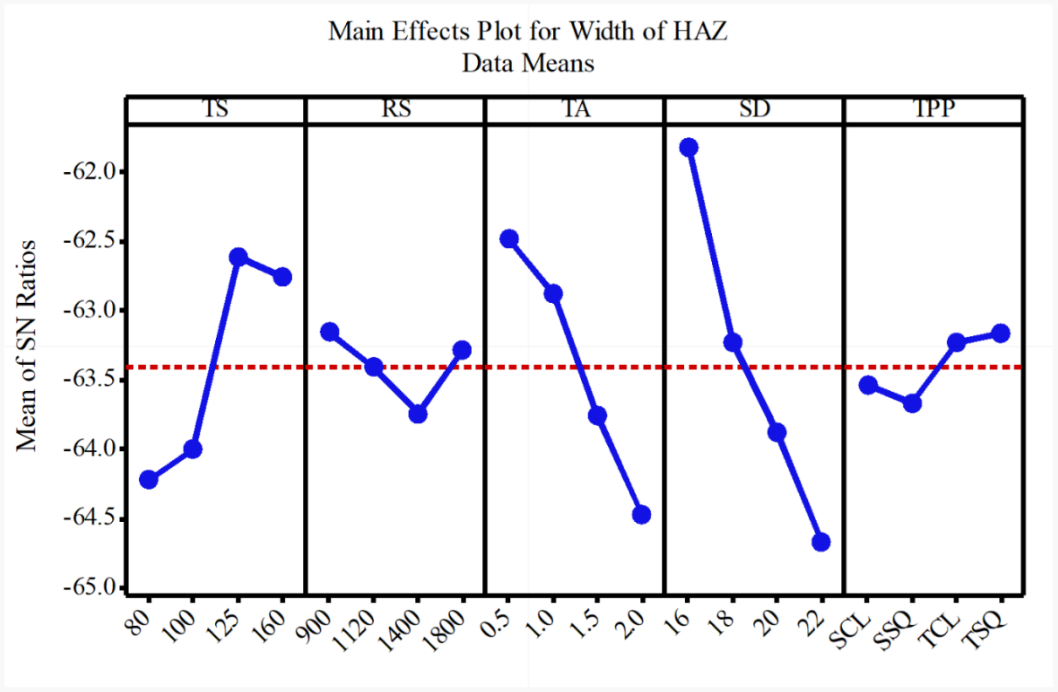

Figure 9. Effects of heat affected zone width for S/N ratios

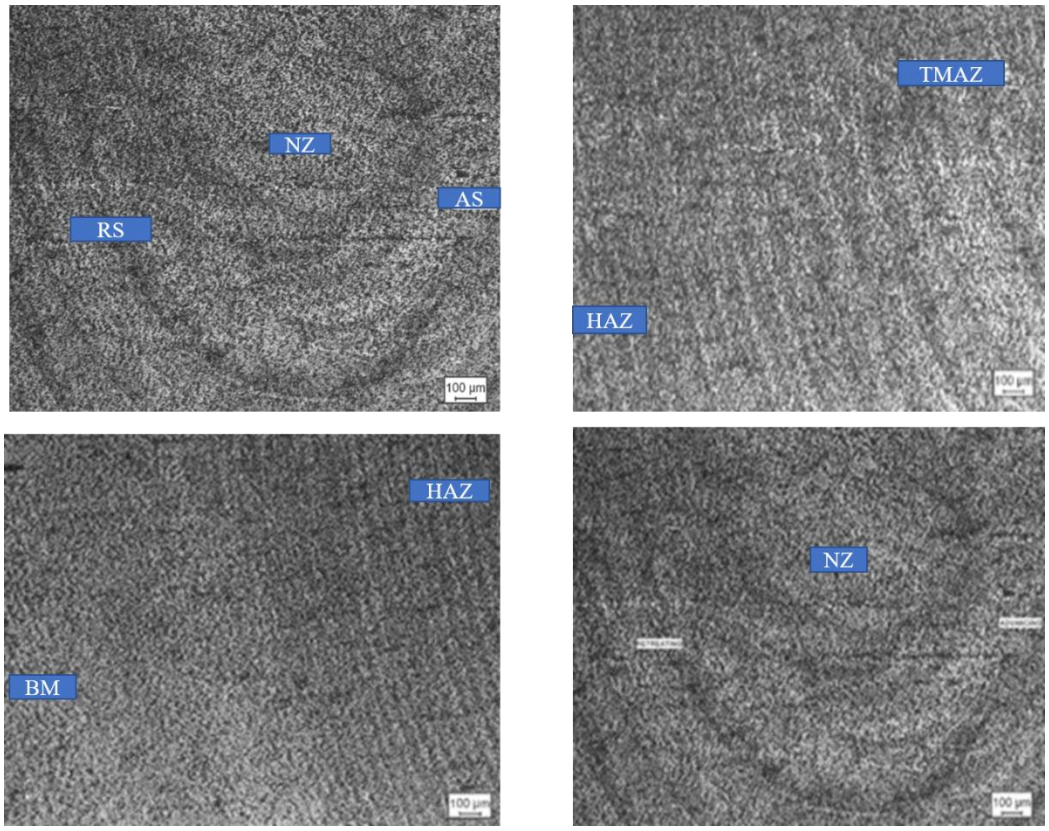

Figure 10. Overview of microstructure (100µm, 5×)

ssTable 1. Process parameters including levels

S.NO	PARAMETER	RANGE			
		LEVEL 1	LEVEL 2	LEVEL 3	LEVEL 4
1	Traverse Speed in MM/MIN	80	100	125	160
2	Rotational Speed in RPM	900	1120	1400	1800
3	Shoulder Diameter in MM	16	18	20	22
4	Tilt Angle in Degree	0.5	1	1.5	2

Table 2. Chemical structure of AA2050 with % weight

Si	Mg	Cu	Li	Fe	Ti	Zr	Zn	Al	Mn	Ag
0.0354	0.358	3.53	0.85	0.0511	0.0375	0.0868	0.0328	94.2	0.345	0.363

Table 3. L_{16} multi-response results

RUN	TS	RS	TA	SD	TPP	Ultimate Tensile Strength (MPa)	Yield Strength (Mpa)	Elongation (%)	Weld Zone Hardness	HAZ Hardness	Bending Load (N)	HAZ Width µm
1	80	900	0.5	16	SCL	297.681	232.971	2.341	108.256	111.252	1560	1206.5072
2	80	1120	1	18	TCL	256.432	183.515	2.408	103.55	112.1	13830	1473.6592
3	80	1400	1.5	20	SSQ	226.391	203.372	3.225	102.752	114.752	1260	1923.0061
4	80	1800	2	22	TSQ	229.883	212.743	2.284	96.53	107.3	1840	2046.5022
5	100	900	1	20	TSQ	287.111	242.055	2.422	105.754	113.5	2560	1492.9221
6	100	1120	0.5	22	SSQ	250.569	214.182	4.261	102.58	116.252	1660	1707.16
7	100	1400	2	16	TCL	260.452	239.512	1.866	106.7	110.251	1540	1527.4955
8	100	1800	1.5	18	SCL	240.201	201.468	2.343	104.52	109.756	1380	1624.7891
9	125	900	1.5	22	TCL	263.963	214.191	2.525	102.753	113.6	1460	1555.6032
10	125	1120	2	20	SCL	316.601	277.304	3.582	103.52	110.751	1240	1644.823
11*	125	1400	0.5	18	TSQ	215.245	203.975	2.084	100.55	110.52	2080	1207.7842
12	125	1800	1	16	SSQ	202.078	185.921	2.482	105.1	113.751	1180	1080.0645
13	160	900	2	18	SSQ	338.881	270.063	3.861	110.3	119.255	1660	1529.4593
14	160	1120	1.5	16	TSQ	312.363	277.941	2.043	107.52	115.1	2660	1163.5384
15	160	1400	1	22	SCL	287.222	249.112	3.284	103.55	112.5	1580	1582.5492
16	160	1800	0.5	20	TCL	189.941	159.081	1.841	102.251	109.6	1360	1263.3431

Table 4. Generating data in a greyscale

RUN	Elongation	Yield Strength	Tensile Strength	Hardness of HAZ	Hardness of weld zone	Width of HAZ	Bending Load
1	0.20661	0.6216	0.7233	0.34693	0.8703	0.86916	0.25675
2	0.23140	0.2055	0.4464	0.40816	0.51851	0.59273	0.13513
3	0.57024	0.3726	0.2447	0.63265	0.46296	0.12778	0.05405
4	0.18181	0.4514	0.2681	0	0	0	0.44594
5	0.23966	0.6980	0.652	0.48979	0.68518	0.572803	0.93243
6	1	0.4635	0.407	0.7551	0.444	0.35118	0.32432

7	0.00826	0.6766	0.4734	0.26530	0.70370	0.53703	0.24324
8	0.20661	0.3565	0.3374	0.2244	0.59259	0.43635	0.13513
9	0.28099	0.46365	0.4969	0.48976	0.46296	0.50794	0.18918
10	0.7190	0.99461	0.8504	0.30612	0.51851	0.41563	0.04054
11	0.09917	0.37767	0.16986	0.28571	0.29629	0.86784	0.6081
12	0.26446	0.22581	0.08144	0.551	0.6296	1	0
13	0.83471	0.9337	1	1	1	0.53499	0.32432
14	0.08264	1	0.82194	0.65306	0.81481	0.91362	1
15	0.59504	0.75744	0.65314	0.40816	0.51851	0.48006	0.27026
16	0	0	0	0.16326	0.42592	0.81035	0.12162

Table 5. Deviation sequences

RUN	Elongation	Yield Strength	Tensile Strength	Hardness of HAZ	Hardness of weld zone	Width of HAZ	Bending Load
1	0.79338	0.37834	0.27662	0.65306	0.1296	0.13083	0.74324
2	0.76859	0.79446	0.55357	0.59183	0.48148	0.40726	0.86486
3	0.42975	0.62737	0.75527	0.36734	0.53703	0.87221	0.94594
4	0.81818	0.54854	0.73183	1	1	1	0.55405
5	0.76033	0.30195	0.3475	0.51021	0.31481	0.42719	0.06756
6	0	0.53642	0.5929	0.24489	0.55555	0.64881	0.67567
7	0.99173	0.32332	0.52658	0.73469	0.29629	0.46296	0.75675
8	0.79338	0.64344	0.66254	0.7755	0.40741	0.56364	0.86486
9	0.71901	0.53634	0.50302	0.51020	0.53703	0.49205	0.81081
10	0.28099	0.00538	0.1495	0.69387	0.48148	0.58436	0.95945
11	0.90082	0.62232	0.83013	0.71428	0.70371	0.13215	0.39189
12	0.73553	0.77418	0.91855	0.4489	0.3703	0	1
13	0.16528	0.06629	0	0	0	0.4651	0.67567
14	0.91735	0	0.17805	0.34693	0.18518	0.08637	0
15	0.40495	0.24255	0.34685	0.59183	0.48148	0.51993	0.7297
16	1	1	1	0.83673	0.57407	0.18964	0.87837

Table 6. Grey relational co-efficient and position of grey relational grades

RUN	Elongation	Yield Strength	Tensile Strength	HAZ Hardness	Weld Zone Hardness	HAZ Width	Bending Load	Weld Quality	Overall Weld S/N Ratio	RANK
1	0.38658	0.56925	0.64381	0.43362	0.79411	0.7926	0.40217	1.6236	4.20941	3
2	0.39413	0.3862	0.47457	0.45794	0.50943	0.5511	0.36633	1.2146	1.688277	12
3	0.53777	0.4435	0.3983	0.57647	0.48214	0.36437	0.34579	1.1808	1.443449	14
4	0.3793	0.47685	0.40589	0.33333	0.33333	0.33333	0.47435	1.0285	0.243287	16
5	0.39672	0.62347	0.58991	0.49494	0.61363	0.53926	0.88095	1.6089	4.130742	4
6	1	0.48242	0.45746	0.67123	0.47368	0.43523	0.42528	1.3405	2.544231	9
7	0.3351	0.60729	0.487049	0.40495	0.62790	0.51922	0.39784	1.3617	2.681741	7

8	0.38658	0.43727	0.430089	0.392	0.551	0.47008	0.36633	1.1853	1.476054	13
9	0.41016	0.48246	0.49849	0.49494	0.48214	0.50400	0.38144	1.267	2.009527	10
10	0.64021	0.98934	0.76971	0.41880	0.50943	0.46109	0.34259	1.5974	4.068942	5
11	0.35693	0.4455	0.3759	0.41176	0.41538	0.79094	0.56061	1.2477	1.918377	11
12	0.40468	0.3924	0.35247	0.52688	0.57446	1	0.33333	1.3525	2.620076	8
13	0.75155	0.8829	1	1	1	0.51813	0.42528	2.2518	7.049152	1
14	0.3527	1	0.73739	0.59036	0.7297	0.8526	1	2.0909	6.404558	2
15	0.55251	0.67335	0.590422	0.45794	0.50943	0.49027	0.40659	1.4056	2.953949	6
16	0.33333	0.33333	0.33333	0.37404	0.46551	0.72501	0.36274	1.1067	0.879174	15

Table 7. Validation examination

Optimum Process Parameters					**Expected Total weld quality**	**Optimal Testing in Total Weld Quality**	**% Error**	**Total Weld Quality under Initial Design**	**% Expansion**
TS	RS	TA	SD	TPP	2.383779	2.284039	4.37	1.9183779	19.06
160	900	2	16	SSQ					

Biography:

Appasaheb N. Pandav is currently serves as the Assistant Controller of Examinations at Amity University Maharashtra, Mumbai and is a research scholar at Visvesvaraya Technological University (VTU) Belagavi. His research is conducted at JCE Belagavi Karnataka, where he focuses on the field of Design and Manufacturing. He has published articles in international journals and has presented his work at an international conference.

Ratan A. Patil is an Associate Professor at JCE Belagavi affililated to Visvesvaraya Technological University (VTU) Belagavi. He conducts his research at, Karnataka, and holds a PhD from VTU Belagavi. His research has been published in both national and international journals, with his primary area of interest being structural dynamics.

Suman Pandipati is an Assistant Professor at Aditya institute of technology and management, Tekkali, Srikakulam Dist, Andhra Pradesh, India. He received his PhD from Centurion University, odisa-India. suman's publications have appeared in national and international journals. The areas of his research interest include Design and manufacturing.